Usage of a Diffractive Optical Element (DOE) for best focal plane estimation of a camera during the integration process

Martin Pertenais, Conor Ryan, Selene Rodd-Routley, Denis Griessbach

Martin Pertenais, Conor Ryan, Selene Rodd-Routley, Denis Griessbach, "Usage of a Diffractive Optical Element (DOE) for best focal plane estimation of a camera during the integration process," Proc. SPIE 12188, Advances in Optical and Mechanical Technologies for Telescopes and Instrumentation V, 121883Z (30 August 2022); doi: 10.1117/12.2627673

SPIE.

Event: SPIE Astronomical Telescopes + Instrumentation, 2022, Montréal, Québec, Canada

Usage of a Diffractive Optical Element (DOE) for best focal plane estimation of a camera during the integration process.

Martin Pertenais[a], Conor Ryan[a], Selene Rodd-Routley[a], and Denis Griessbach[a]

[a]German Aerospace Center (DLR), Institute of Optical Sensor Systems, Rutherfordstr. 2, 12489 Berlin, Germany

ABSTRACT

Diffractive Optical Elements (DOEs) are commonly used in the photonics community for several purposes, such as geometrical calibration of cameras,[1] medical treatments, lithography, LIDAR applications. In the context of the optical alignment and integration of the RAman Spectrometer for MMX (RAX),[2] a DOE was included in the test setup with the goal of providing a clear figure of merit to optimize the focusing of a dioptric lens objective on to the spectrometer detector. This Raman spectrometer will be integrated later this year in a small Rover on-board the Martian Moons eXploration (MMX) mission led by JAXA, and will operate on Phobos' surface to characterize the different materials composing Phobos' soil. To achieve this, the optical design of RAX is very challenging in terms of performance to reach in very limited volume and mass. As described in Ref. 2, the optical alignment and integration of RAX was a very challenging exercise, requiring several optical setups and methods. The usage of a DOE was introduced to solve a classical problem during the integration of a camera: how to integrate both the optical objective (lens assembly) and the detector to ensure that both the optical focal plane and the detector sensitive plane are co-planar. When illuminated by a collimated laser beam, the implemented DOE generates a regular pattern of collimated beams with well-known deviation angles from the input beam. It acts as a 2D diffraction grating, and generates a pattern field which covers the entire field of view of our camera. Thanks to this property, the Camera Interface Objective of RAX could be successfully positioned and oriented with respect to the detector mechanical interface. It was achieved by acquiring successive images of the DOE pattern with controlled defocused laser beam illuminating it. We were then able to compute the equivalent mechanical defocus needed to maximize the image quality. This maximizes the overall instrument performance and will ensure best possible scientific measurement on Phobos.

Keywords: AIT, Raman, DOE, Focusing, Optical Integration, MMX, RAX

1. INTRODUCTION AND CONTEXT

1.1 Best Focal Plane Estimation Problematic

The problematic of integrating a detector at the best focal position with respect to the optical system is well-known in the space instrument community. The first step in this process is generally to clearly define a merit function determining what is actually this best focus position. For a spectrometer, this merit function may be the spectral resolution achieved on the detector. For an extended scene imager, the measurement of the Modulation Transfer Function or the contrast of an image is another candidate, while for point source imagers or photometers, the Point-Spread-Function (PSF) characterization is the most common method. For example, for the PLATO exoplanet-hunting Mission, the best focus position for each Camera is determined by characterizing the PSF size of a point-source (simulating a star) at different field of view positions.[3] The detailed merit function is this case is the Ensquared Energy Fraction (EEF) of each PSF within a given number of pixel size (e.g. a square of 3x3 pixels).

Such measurements have however the main drawback to be time-consuming and complex in terms of laboratory setup. Indeed, in order to reach several field of view positions, the camera (or the light source) needs to be rotated in a precise, controlled and repeatable manner. This includes generally the use of a gimbal or hexapod system.

Further author information: Send correspondence to martin.pertenais@dlr.de

Advances in Optical and Mechanical Technologies for Telescopes and Instrumentation V, edited by Ramón Navarro, Roland Geyl, Proc. of SPIE Vol. 12188, 121883Z
 · 0277-786X · doi: 10.1117/12.2627673

To overcome this drawback, we propose the use of a Diffractive Optical Element (DOE), introduced in more details in section 1.2. This allows the illumination of the sensor with a pattern of points covering the complete field of view in a single snapshot without needing any rotation system. The setup required is the same as the one used to performed the geometric calibration of a camera with a DOE, as was for example done for MERTIS on BepiColombo and explained in Ref. 4.

1.2 DOE Concept

Diffractive optical elements can be used to perform an amplitude-division on an incoming monochromatic beam with wavelength λ, creating a number of beams with well-known propagation directions. As the image on the sensor is a Fraunhofer diffraction pattern, each projected image point represents a point at infinity, denoted in 3D projective space $\mathbb{P}^3$ by the homogeneous coordinate $\mathbf{d} = \left[X, Y, Z, 0\right]^T$ with

$$\mathbf{d} = \left[\lambda f_x,\ \lambda f_y,\ \sqrt{1 - \lambda^2(f_x^2 + f_y^2)},\ 0\right]^T \tag{1}$$

where $\mathbf{f} = [f_x, f_y]$ denotes a spatial frequency encoded in the DOE. With suitable computational algorithms[5] it is possible to encode spatially aperiodic DOEs with arbitrary spatial frequencies, choosing the propagation directions freely. As they are easier to design for the large aperture diameters needed, a spatially periodic DOE was used here. Its spatial frequency is given by $f_{x,y} = n_{x,y}/g_{x,y}$, with grating constants $[g_x, g_y]$ and $[n_x, n_y]$ denoting the particular diffraction orders. The grating vectors are defining the $x-$ and $y-$axes of the DOE reference frame. However, eq. (1) is only valid if the incident light wave is a plane wave with uniform intensity distribution, perfectly perpendicular to the DOE surface. In a real setup, the beam is finite in extension and often has a non-uniform intensity profile, which is typically Gaussian. Moreover, a slight tilt of the DOE with respect to the incident beam is hard to avoid. As we will see later on, this tilt has however no significant impact on the size of the spots, which is what matters for this particular application.

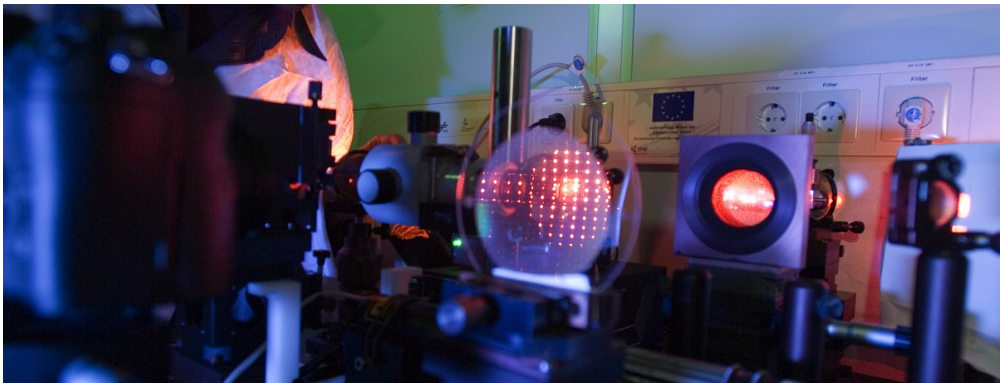

Figure 1. Exemplary setup with laser source, DOE and camera

The deviations of the real beam profile from a plane wave cause the diffraction spots in the far field to have a certain size, which can be estimated from the Convolution theorem of Fourier Optics.[6] The consequent propagation directions are determined with the diffraction formula for non-perpendicular incidence to the DOE. For the following analysis, the DOE reference system will be used, in which the incident beam is given by

$$\mathbf{r} = \left[\sin(\beta), -\sin(\alpha)\cos(\beta), \cos(\alpha)\cos(\beta)\right]^T \tag{2}$$

with the Euler angles α and β rotating the $x-$ and y-axes of the DOE reference frame w.r.t. the collimator reference frame. The directions of the diffracted beams are now obtained as follows[7]

$$\mathbf{d} = \left[\lambda f_x + r_x, \lambda f_y + r_y, \left(1 - (\lambda f_x + r_x)^2 - (\lambda f_y + r_y)^2\right)^{1/2}, 0\right]^T . \tag{3}$$

As seen with eq. (3), it is in principle no problem to use wavelengths on a DOE, that are different than the wavelength it has been optimised for. The directions of the diffracted beams will then be different, but will

still create a regular pattern of beams. It is straightforward to calculate the diffracted beam directions in the DOE reference frame by simple matrix operations. In order to transform the beam directions into the camera reference frame, the exterior orientation of the camera w.r.t. the DOE reference frame has to be considered with

$$\mathbf{d}' = \begin{bmatrix} \mathbf{R} & \mathbf{t} \\ 0 & 1 \end{bmatrix} \mathbf{d}, \tag{4}$$

where $\mathbf{R}$ is a 3×3 rotation matrix defining the camera orientation and $\mathbf{t}$ the translation vector for the camera position. Equation (4) shows that the mapping of ideal points at infinity is invariant against translation.

1.3 MMX Mission and RAX Instrument

The Martian Moons eXploration (MMX) mission led by the Japanese Space Agency JAXA will conduct remote sensing of both Martian moons Phobos and Deimos and in-situ observations and return samples from Phobos.[8,9] A small rover will be operating on Phobos' surface and perform scientific measurements, in particular with its RAman Spectrometer for MMX (RAX). The instrument is jointly developed by DLR with partners from Spain (University of Valladolid, INTA) and Japan (University of Tokyo and JAXA). The primary objective of the RAX instrument is the investigation of the surface mineralogy on Phobos by spectral identification using Raman spectroscopy.[10]

The Spectrometer Module of RAX is a very compact optical assembly allowing both to focus the Raman excitation laser (fiber-fed) onto Phobos' surface and to gather the Raman signal emitted by the minerals on the surface and image a spectrum of it. Figure 2 shows a schematic view of RAX optical design.

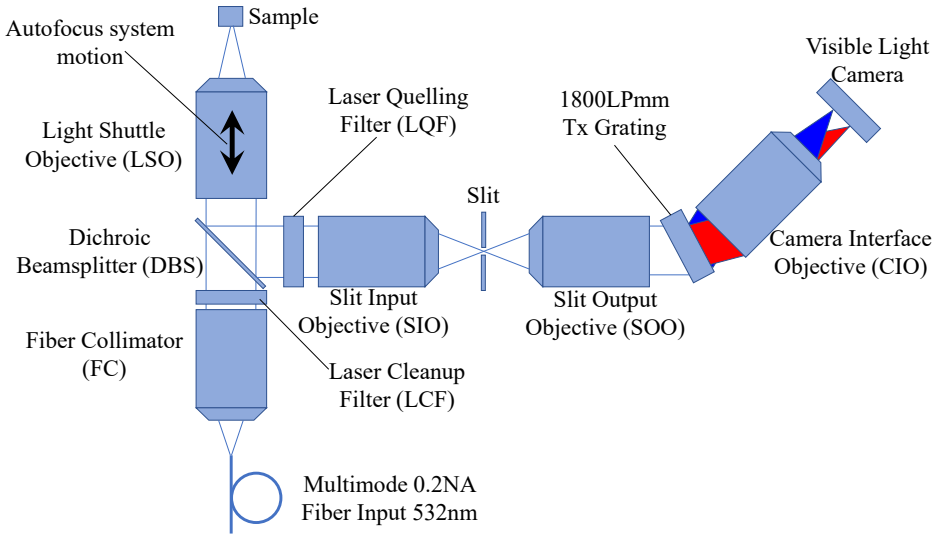

Figure 2. Schematic description of the optical design of RAX[11]

The DOE method was applied to correctly integrate the Camera Interface Objective (CIO) to the CMOS Detector used to create the image of the Raman Spectrum.

2. APPLICATION ON RAX CAMERA

2.1 RAX Camera Interface Objective

The 0.24NA Camera Interface objective takes the system grating output as its input. That is, it accepts collimated beams of different wavelengths and directions and maps them into focussed spots on the Camera CMOS chip. The Camera Interface Objective accepts collimated beams, each of diameter 14.2 mm, with input directions ranging from -10° to +10°. The beam wavelength varies linearly with input angle so that the -10° beam has a wavelength of 532nm and the +10° beam a wavelength of 680nm. With these specifications, the

objective's focal length is 29.6 mm and the 532 nm $\leq \lambda \leq$ 680 nm spectral range is mapped onto a line on the camera ranging over $\pm$5.16 mm. Figure 3 shows the opto-mechanical design of the CIO, including 7 lenses and telecentric output beams on the left hand side.

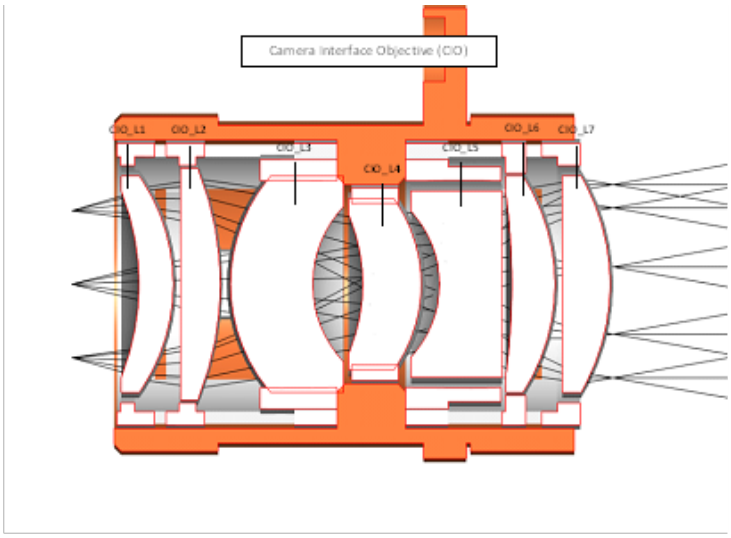

Figure 3. Opto-mechanical Design of the Camera Interface Objective (CIO) of RAX.

RAX focal plane assembly consists of the 3D-Plus 3DCM734-1 CMOS camera module. It contains both the 4 Megapixels CMOS detector itself and the digital processing unit. It is visible as the gold part of fig. 4. This was mounted onto a bracket in a way that provided lateral position adjustments of the detector sensitive surface as well as simple and repeatable integration in the RAX housing. The other adjustable degrees of freedom between the CIO and detector assembly were the axial position of the CIO and the tip/tilt orientation of the CIO. These were controlled by shimming in a "Maxwell" kinematic mount, consisting of three sphere-in-V-groove interfaces separated by 120 degrees about the optical axis. The spherical surfaces were attached to the CIO at the end of each radial "arm", while the grooves were machined into the rectangular bracket bearing the detector. The sphere/groove interfaces were pressed together by screws passing through the middle each sphere/groove interface. As the spherical washers are not monolithic with the CIO, mechanical tolerances were minimised to reduce clearance around the washer. Although separation of the CIO from the focal plane assembly was required to laterally adjust the detector sensitive surface, the repeatability of the designed kinematic mount allowed the same CIO position and orientation were achieved upon CIO re-integration. As seen in fig. 4, all optomechanical components in the RAX spectrometer were blackened with coatings, tested for ultra-low laser scattering and Fluorescence emission.[12]

2.2 Test Setup

The idea of the test is to illuminate the DOE placed just in front of the CIO with a collimated laser beam in order to create a pattern of PSFs on the detector across the complete CIO field of view.

The DOE we use was optimized to work for λ = 633 nm and produces a pattern of 7x7 points with 4° angular separation between each point. The 633 nm laser used was fed into the setup with a multimode fiber placed on the focal plane position of a microscope objective creating the collimated beam. The fiber output was placed on a translation stage allowing the operator to control the focus position of the laser with respect to the collimator. A Shack-Hartmann sensor was used after the collimator to properly place the fiber output in order to create the best collimated beam possible. The setup is presented in fig. 5.

After the laser has been properly collimated, the next step is to align the optical axis of the Camera (CIO + detector) with the collimated laser beam. This is done by acquiring images of the collimated beam and minimizing the easily detectable coma of the spot (image of the fiber output) visible on the image. The DOE

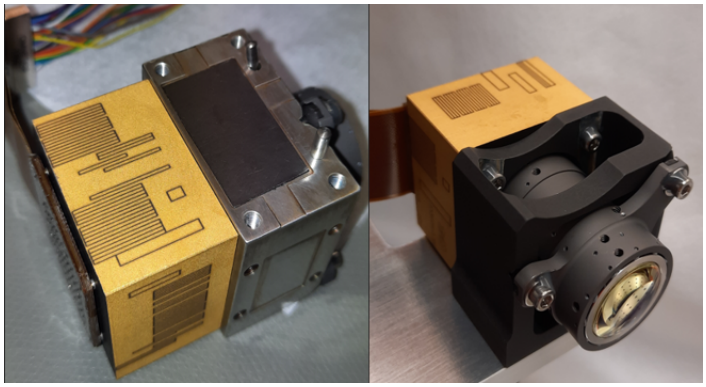

Figure 4. Photo of the CIO integrated on the CMOS detector assembly.

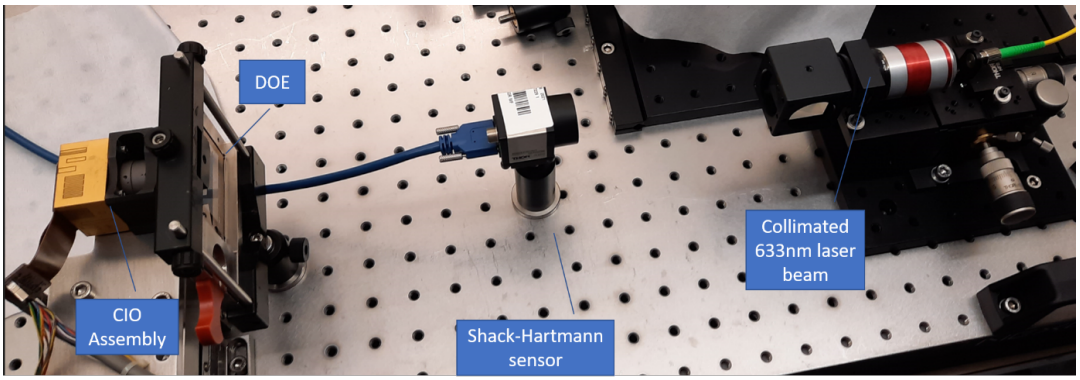

Figure 5. Picture of the setup in the laboratory used for the DOE best focus estimation.

can then be placed in front the camera, as close as possible to the entrance pupil in order to minimize the vignetting of the outer diffraction points entering with the greatest angle. Figure 6 shows an example of image acquired with the camera and the DOE placed in front of it. The 0th diffraction order is well aligned with the optical axis and is imaged in the center of the detector. A pattern of ± 2 points around the 0th order is visible. Due to vignetting, the 4 points in the corners are not visible.

In this particular case, the DOE surface is much larger than the entrance pupil. Therefore the absolute X/Y position of the DOE with respect to the camera is irrelevant. The rotational position of the DOE with respect to the optical axis is also irrelevant for us as the size of the spots created by the diffraction effect is independent from the incident angle. The only downside of having the DOE not perfectly orthogonal to the optical axis is in term of radiometry with a decreased diffraction efficiency. In order to verify this, a repeatability test has been performed and is presented in the next section.

3. MEASUREMENTS AND RESULTS

The test plan with this setup is to defocus in a controlled way the collimated laser beam illuminating the DOE. This is done by translating the output of the laser fiber at the entrance of the collimator. Using the Vernier scale of the translation stage, the physical defocus applied can be known very precisely. For each defocus step, the focus quality is estimated with a given merit function estimating the PSF size. Using the longitudinal magnification between the entrance of the collimator and the detector (square ratio of the focal lengths), the best focus position estimated can be converted into a physical defocus between the CIO and the detector. This gap can then be corrected by shims to bring the detector on the optical best focus position.

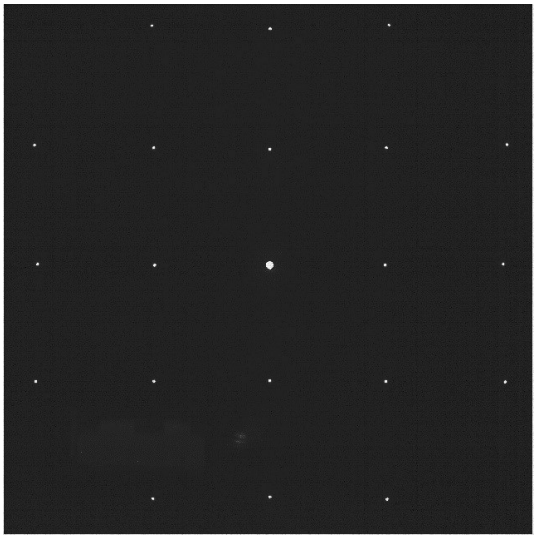

Figure 6. Example of an image acquired with the Flight Model Camera of RAX of a collimated laser beam seen through the DOE.

3.1 Image Acquisition and Processing

The definition for the best focus merit function in this study case was chosen to be the average Ensquared Energy Fraction (EEF) in 3x3 pixels. The image of each spot creates a PSF on the detector that spreads the light into several pixels. When the detector is at the best focus position of the optical objective, the PSF is the smallest possible and the fraction of light enclosed in a fixed number of pixels (in this case 3x3) is then maximized. In practise, an analyses script was developed to process the images acquired. The steps performed by the script are the following:

- Open and read the signal image
- Open and read the background images (with laser turned off)
- Subtract the median background from the signal image
- Identify the 20 spots of interests in the pre-processed image
- Identify for each spot the 3x3 macro-pixel providing the highest flux
- Compare this integrated flux to the reference, being the integrated flux of 12x12 pixels around each spot.
- Plot a field of view map of this EEF in 3x3 pixels and save the average value across the field of view.

In order to verify the statement made earlier on the DOE position with respect to the Camera, and make sure that we don't need to create a setup positioning it with more precision, a repeatability test was performed. It also enabled us to have first estimate of the error bars of the measurement due to the setup itself and the processing script. For a fixed focus position, an image was acquired and the average EEF over all spots in 2x2 and in 3x3 pixels computed. The DOE was then physically removed from the setup and placed again by hand in a similar position. This was done in total 11 times.

Figure 7 shows the result of the EEF in 2x2 pixels (blue points) and in 3x3 pixels (orange points). The result of this repeatability test shows a standard deviation of the 2x2 pixels measurement of 1.6% and 0.5% for 3x3 pixels.

This is excellent result confirming the very small, if not negligible, dependency of the measurement to the absolute position of the DOE with respect to the camera. The highest error bar on the measurement with 2x2

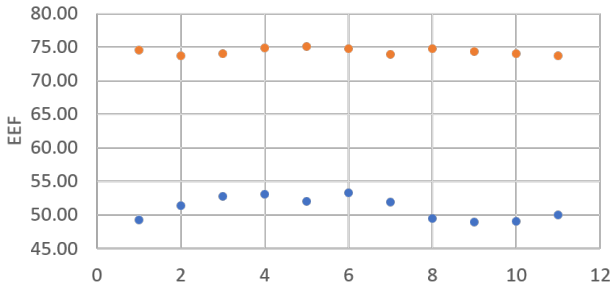

Figure 7. Average Ensquared Energy Fraction in 2x2 pixels (blue) and 3x3 pixels (orange) measured 11 times with 11 slightly different DOE positions.

pixels is explained by the fact that when looking at a small region (2x2 pixels) compared the PSF size, the measurement is much more dependent on the PSF centroid sub-pixel position. This is the main reason why the EEF in 3x3 pixels was used for the actual calibration and not 2x2 pixels.

3.2 Best Focus Determination

The test was then performed, using the fine screw of the translation holding the laser fiber at the entrance of the collimator. After proper focusing of the collimator, this fine screw offered a range of ±2 rotations in each direction (ClockWise and AntiClockWise).

The first iteration of measurement provided an unexpected result: the PSF size field of view map showed very large PSF across the complete FoV with EEF in 3x3 pixels of around 15%, while more than 80% is expected around the best focus. This meant that we were very far for the best focus position. By defocusing the collimated laser beam in both direction, the merit function increased significantly after 2 fine rotations in the clock-wise direction and brought the average EEF in 3x3 pixels up to 20%. With a fine rotation being a displacement of 50 µm and a longitudinal magnitude of 4, these 2 rotations corresponded to a defocus between the CIO and the detector of 25 µm. The 20% being still very far away from the expected performance, we suspected the best focus position to be much further away and decided therefore the remove the 100 µm shims positioned at the mechanical interface between the CIO and the detector, and repeat the measurement. After removal of the shims, re-integration of the CIO to the detector and alignment of the setup, the test was repeated and provided the results shown in fig. 8.

This measurement was performed using the coarse screw of the translation stage instead of the fine one, which is less precise but with a much wider range. The results present a significant increase of our merit function and smallest PSF for a defocus between 0.8 and 1 coarse clock-wise rotation. A coarse rotation corresponds to a physical translation of 500 µm of the focus of the fiber collimator, or 125 µm between the CIO and the detector. Figure 9 shows the evolution of the field of view maps for the 4 focus points also plotted in fig. 8.

The conclusion from this test is that there still is a defocus of 100 to 125 µm between the detector and the CIO. As the defocus is in the negative direction, the CIO is 100 to 125 µm too far away from the detector sensitive area. The optomechanical design assumed 100 µm would be more than enough adjustment range to compensate manufacturing and assembly tolerances. So the defocus cannot be fully removed by removing shims.

The solution chosen was to remove approximately 150 µm from the three spherical washers in the kinematic mount, and then add corresponding shims if necessary.

3.3 Final Focus Verification

After the 3 interface pieces were milled down to remove 150 µm of material, the CIO was integrated again to the detector and re-aligned to the setup.

The test was then repeated with a collimated beam and with small focus variation around the optimal collimation. The result was excellent and showed a constant (within error bars) PSF size across the field of view for defocus of ±25 µm in both directions. Figure 10 shows the comparison between the performance achieved

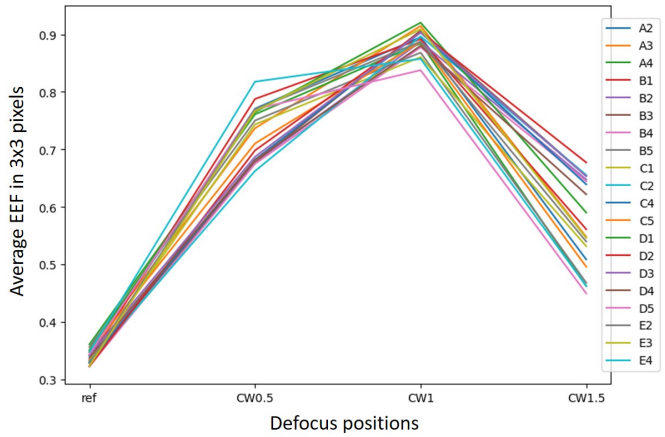

Figure 8. Ensquared Energy Fraction in 3x3 pixels for the 20 relevant field of view positions (A-E being the columns left to right and 1-5 the lines top to bottom of the pattern of point) and different focus positions. "Ref" corresponds to the collimated laser beam, while "CW.." corresponds to the Clock Wise rotations of the coarse screw of the translation stage.

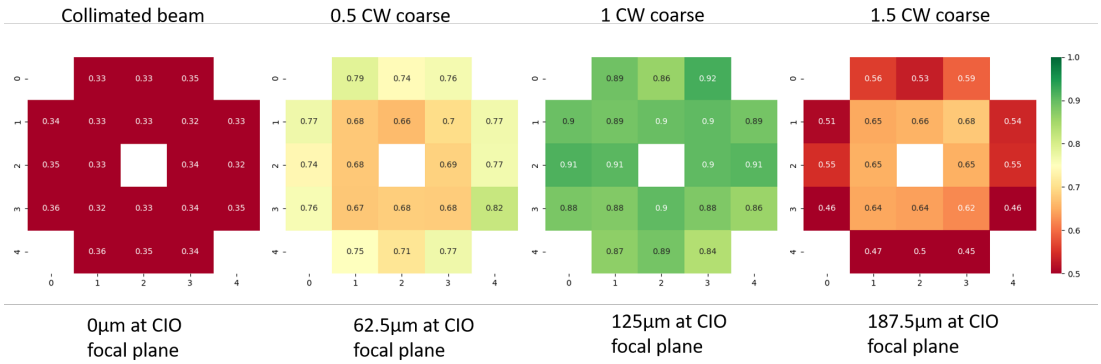

Figure 9. Ensquared Energy Fraction field of view maps for several focus positions. Conclusion: there is a defocus of 100-125 µm between the detector and the CIO.

for a perfectly collimated beam with the nominal mechanical interface on the left-hand side, the performance achieved with a strong collimator defocus, and the achieved performance on the Flight Model with the new mechanical interface and a perfect collimated beam.

As shown by the field of view map, the results achieved are very similar to one simulated by a strong defocus and provide very small PSFs with Ensquared Energy Fraction in 3x3 pixels largely above the 80% anticipated by design at the best focus position. With this, we have the confirmation that the detector and the CIO are now in their correct relative position along the optical axis, and the retaining screws can now be glued in place for their flight configuration.

3.4 Method Validation with Spectrum

As this is the first time we used a DOE to perform a best focus estimation calibration on a space instrument, we cross-validated it with a more standard method.

For this, a spectrum simulation station was developed and is basically a homemade spectrometer. It creates a spectrum in the same wavelength range as the instrument (RAX in this case) and with the same geometrical characteristics. Only the spectral resolution is different due to the different slit size. As with the DOE setup, it provides the capability to control the defocus of the incoming beam. Before the hemispherical washers were

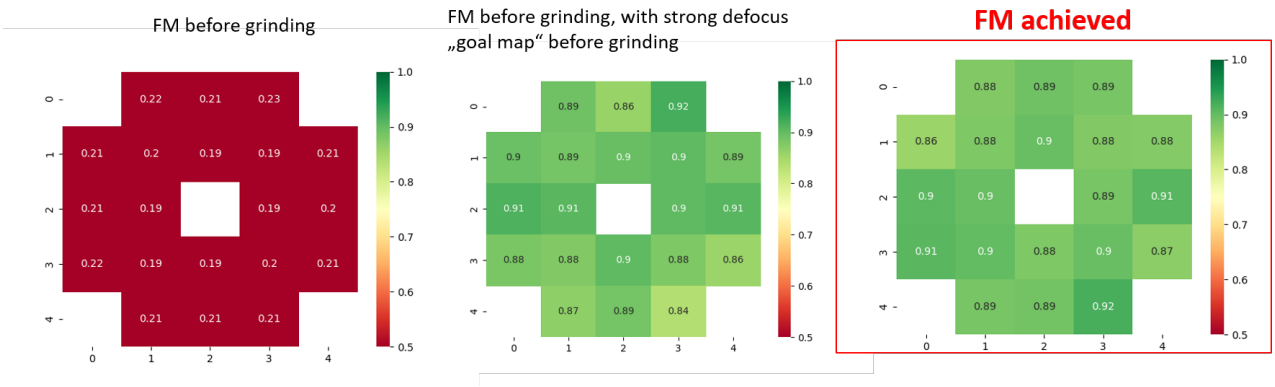

Figure 10. Comparison of the EEF maps before grinding the mechanical interfaces and the achieved one afterwards.

milled, the defocus was measured with this setup to confirm the DOE findings. The measured spectra for 3 cases are presented in fig. 11. The blue spectrum corresponds to a fully collimated beam, while the orange and green ones correspond respectively to an equivalent of 50µm and 100µm defocus of the CIO.

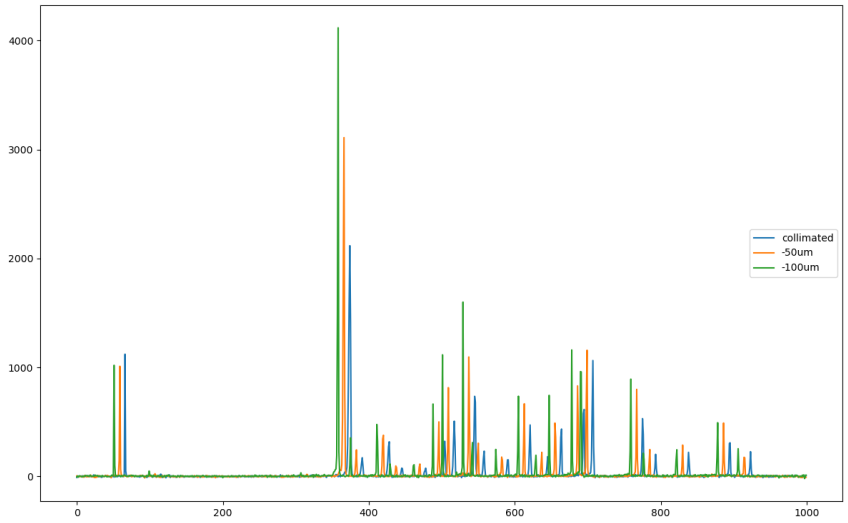

Figure 11. Measured spectra for 3 cases: blue with a collimated beam, orange and green with an equivalent defocus of respectively 50 and 100 µm of the CIO.

The intensity of the lines provides us direct insight of the spectral resolution achieved, which is directly linked to the correct positioning of the detector in the focal plane of the CIO. This confirmed the results from the DOE and gave the final green light for milling down the parts.

After the re-integration of the CIO with the shorter washers and verification on the DOE, some spectra were acquired again with this setup and confirmed again that the plateau of best focus has been reached.

4. CONCLUSION AND OUTCOME

As presented in this paper, the use of a Diffractive Optical Element can be a very efficient, accurate and practical way to perform the best focus integration of cameras for space instruments. Compared to more standard methods used for similar tests, and involving the use of an hexapod or gimbal, this method offers the possibility to reach similar results with a much simplified and robust setup. The only moving part needed is a translation stage to control the defocus of the incoming light. One limitation of this method is that is works only with monochromatic light. For very chromatic instruments working in broadband applications, the test would have to be repeated for several wavelength and the measurement recombined into an equivalent polychromatic PSF.

REFERENCES

[1] Bauer, M., Grießbach, D., Hermerschmidt, A., Krüger, S., Scheele, M., and Schischmanow, A., "Geometrical camera calibration with diffractive optical elements," *Opt. Express* **16**, 20241–20248 (Dec 2008).

[2] Pertenais, M., Ryan, C., Routley, S., Rockstein, S., Schrandt, F., Hagelschuer, T., Gutruf, S., Buder, M., Boettger, U., Schroeder, S., Moral, A., Prieto-Ballesteros, O., Rull, F., Cho, Y., and Huebers, H., "On the Alignment, Integration and Testing of the RAman Spectrometer for MMX (RAX)," *Proc. SPIE* **XX**, XX (2022).

[3] Pertenais, M., Cabrera, J., Griessbach, D., Erikson, A., Vandenbussche, B., Samadi, R., Reese, D., and Rauer, H., "Overview of PLATO's cameras on-ground and in-orbit calibration and characterisation," **11852**, 97 – 109, International Society for Optics and Photonics, SPIE (2021).

[4] Bauer, M., Baumbach, D., Buder, M., Börner, A., Grießbach, D., Peter, G., Santier, E., Säuberlich, T., Schischmanow, A., Schrader, S., and Walter, I., "MERTIS: geometrical calibration of thermal infrared optical system by applying diffractive optical elements," **9608**, 30 – 37, International Society for Optics and Photonics, SPIE (2015).

[5] Hermerschmidt, A., Krüger, S., and Wernicke, G., "Binary diffractive beam splitters with arbitrary diffraction angles," *Opt. Letters* **32**, 448 – 450 (2007).

[6] Goodman, J. W., [*Introduction to Fourier Optics*], Roberts & Company Publishers, 3rd ed. (2005).

[7] McPhedran, R. C., Derrick, G. H., and Botten, L. C., [*Theory of Crossed Gratings*], 227–276, Springer Berlin Heidelberg, Berlin, Heidelberg (1980).

[8] Ulamec, S., Michel, P., Grott, M., Böttger, U., Hübers, H.-W., Cho, Y., Rull, F., Murdoch, N., Vernazza, P., Biele, J., and Tardivel, S., "The mmx rover mission to phobos: Science objectives," in [*72nd International Astronautical Congress (IAC 2021)*], (Oktober 2021).

[9] Michel, P., Ulamec, S., Böttger, U., Grott, M., Murdoch, N., Vernazza, P., Sunday, C., Zhang, Y., Valette, R., Castellani, R., Biele, J., Tardivel, S., Groussin, O., Jorda, L., Knollenberg, J., Grundmann, J. T., Arrat, D., Pont, G., Mary, S., Grebenstein, M., Miyamoto, H., Nakamura, T., Wada, K., Yoshikawa, K., and Kuramoto, K., "The MMX rover: performing in situ surface investigations on Phobos," *Earth Planets and Space* **74** (Jan. 2022).

[10] Cho, Y., Böttger, U., Rull, F., Hübers, H.-W., Belenguer, T., Börner, A., Buder, M., Bunduki, Y., Dietz, E., Hagelschuer, T., Kameda, S., Kopp, E., Lieder, M., Lopez-Reyes, G., Moral Inza, A. G., Mori, S., Ogura, J. A., Paproth, C., Perez Canora, C., Pertenais, M., Peter, G., Prieto-Ballesteros, O., Rockstein, S., Rodd-Routley, S., Rodriguez Perez, P., Ryan, C., Santamaria, P., Säuberlich, T., Schrandt, F., Schröder, S., Stangarone, C., Ulamec, S., Usui, T., Weber, I., Westerdorff, K., and Yumoto, K., "In situ science on Phobos with the Raman spectrometer for MMX (RAX): preliminary design and feasibility of Raman measurements," *Earth, Planets and Space* **73**, 232 (Dec. 2021).

[11] Rodd-Routley, S. A., Belenguer, T., Böttger, U., Buder, M., Cho, Y., Dietz, E., Hagelschuer, T., Hübers, H. W., Kameda, S., Kopp, E., Moral Inza, A. G., Mori, S., Prieto-Ballesteros, O., Rockstein, S., Rull, F., Ryan, C., Säuberlich, T., Schrandt, F., Schröder, S., Usui, T., and Yumoto, K., "Optical Design and Breadboard of the Raman Spectrometer for MMX-RAX," *Lunar and Planetary Science Conference*, 1923 (Mar. 2021).

[12] Ryan, C., XXX, S., and Böttger, U., "Measurements of black surface treatments for straylight and fluorescence suppression in the RAman Spectrometer for MMX (RAX)," *Proc. SPIE* **XX**, XX (2022).